INTERNAL PRESSURE RESPONSE OF A HUMAN HEAD SURROGATE MODEL SUBJECT TO VARIABLE IMPACT LOADING WITH FINITE ELEMENT ANALYSIS

by

AARON JACKSON

Submitted in partial fulfillment of the requirements
for the degree of Master of Science in Aerospace Engineering at
The University of Texas at Arlington
December 2021

Arlington, Texas

Supervising Committee:

Ashfaq Adnan, Supervising Professor
Alan P. Bowling
Kent Lawrence

DEDICATION

I dedicate this thesis to my loving and supportive family.

ABSTRACT

INTERNAL PRESSURE RESPONSE OF A HUMAN HEAD SURROGATE MODEL SUBJECT TO VARIABLE IMPACT LOADING WITH FINITE ELEMENT ANALYSIS

Aaron Jackson, M.S.

The University of Texas at Arlington, 2021

Supervising Professor: Ashfaq Adnan

Traumatic brain injury (TBI) from blunt impacts to the head is a major cause of brain disease and dysfunction for thousands of people every year. Each year in the United States approximately 1 million TBI cases occur causing as many as 56,000 deaths and leaving nearly 90,000 individuals with long-term disabilities. Damage resulting from a TBI occurs on a multiscale level including the macroscopic, tissue, and neuron length scale. This research focuses on correlating the macroscopic blunt impact conditions to the internal pressure developed in the coup and countercoup for water and gelatin-filled head models. Two separate 3D printed models are studied: the coronal model simulates a frontal impact and the sagittal simulates a side impact. A dynamic impacting test platform was designed and manufactured in-house to deliver varying controlled impact conditions; impact acceleration and velocity are verified via a rigid body dynamics analytical simulation and digital image correlation (DIC). The coup and countercoup

are the measured regions of interest due to the potential for high magnitude transient pressure spikes that may result in cavitation and thus damage the surrounding brain structure. A range of experiments was performed measuring the resulting bulk acceleration and internal fluid pressure response over varying impact conditions for both water and gelatin solutions. The experiment is validated using ANSYS Explicit Dynamics; resulting pressure in the coup and countercoup region are recorded for varying impact velocity conditions. A mesh convergence study was performed for both the coronal and sagittal plane models. The experiment shows that at the maximum impact velocity of 5.5 m/s the coup pressure is approximately +96 kPa while the countercoup is -47.3 kPa. The finite element model shows relatively good agreement with the coronal experimental results for the 5.5 m/s impact condition with a coup pressure of +102 kPa and a countercoup pressure of -68 kPa.

TABLE OF CONTENTS

LIST OF FIGURES

LIST OF TABLES

CHAPTER 1

INTRODUCTION

Traumatic brain injury (TBI) from a blunt or blast impact to the head is a major cause of brain disease and dysfunction for thousands every year. Each year in the United States approximately 1 million TBI cases occur causing as many as 56,000 deaths and 70,000 to 90,000 individuals to develop long-term disabilities [1]. TBI affects a wide variety of individuals including but not limited to our warfighters, victims of automobile accidents, and sports-related injuries. Given there are so many affected, it is a major field of scientific research to understand the damage mechanisms that lead to a TBI and how it can be prevented by establishing injury thresholds and sensing mechanisms. Due to the natural complexity of the human brain, a TBI can be assessed on many different length scales. From a macroscopic point of view, the impacting conditions can be directly related to the bulk acceleration of the head and the internal pressure developed in the CSF layer or white and gray matter regions. Damage can also be assessed on smaller length scales such as the tissue level or the individual neuron and its cytoskeletal components. For a complete picture and understanding of any specific TBI incident, each of these length scales must be understood completely and connected into a holistic framework. Damage criteria framed to consider the entire length scale of a head injury would need to relate this macroscopic, tissue, and neuronal injury together.

This study focuses on understanding the macroscopic characteristics of a surrogate human head model subject to variable impact loading. Several standard models for damage criteria have been established including the Head Injury Criteria (HIC) model, Generalized

Acceleration Model for Brain Injury (GAMBIT), Brain Rotational Injury Criteria (BRIC), and Rotational Injury Criteria (RIC) [2]. In these models only the linear and rotational acceleration of the head is considered; no in-vivo information is understood or considered from these damage assessments. Many of these models have correlated the accelerations felt by the head under impact to the post-incident conditions of the patient. In such methods, there is no understanding of the mechanical deformations or failure of the brain components. Correlating the bulk-head acceleration to the internal pressure developed inside the brain gives a more complete and meaningful picture of the mechanisms that can lead to a brain injury on the macroscale.

This study considers the pressure distribution formed in surrogate human head models when subject to linear acceleration. When a contained fluid is set into motion via an acceleration input, a gradient of compressive and tensile pressure forms within the fluid region. Consider the fluid-filled cuvette in Figure. 1. When a force is applied from the top, a compressive pressure is developed in the end where the force is applied. On the opposite end of the cuvette, a tensile pressure is developed. If the contained fluid is given a sufficient force input, the tensile force in the opposite end of the applied input exceeds the tensile strength of the fluid; the fluid will then tear apart and form temporary cavities known as cavitation [3]. This phenomenon has been demonstrated in several studies that relate the cuvette acceleration to the pressure and cavitation formation [4] [5]. It has been speculated since the 1950's that this same phenomenon applies to head injury. When someone is subject to a blunt impact, the brain region adjacent to the impact site experiences compressive pressure, while the region opposite the impact site develops negative pressure with the potential for cavitating brain fluid. In the case of a brain injury, the violent collapse of the cavitating bubbles in the tensile region has a high potential to damage the near brain structure. The adjacent compressive region is referred to as the coup, and the tensile

region opposite the impact site is referred to as the contrecoup. This is known as a focal injury as the pressure developed in the coup and contrecoup regions are of sufficiently high magnitude in a very localized region. Regardless of the impact orientation or impact plane, the adjacent region is always considered the coup, and the opposite side is the contrecoup. Similar to the cuvette example, the expected intracranial pressure distribution due to an impact to the head is seen in Figure. 2. When the head is set into an accelerated motion the pressure gradient formed in the brain can be directly related to the damage done to the brain structure.

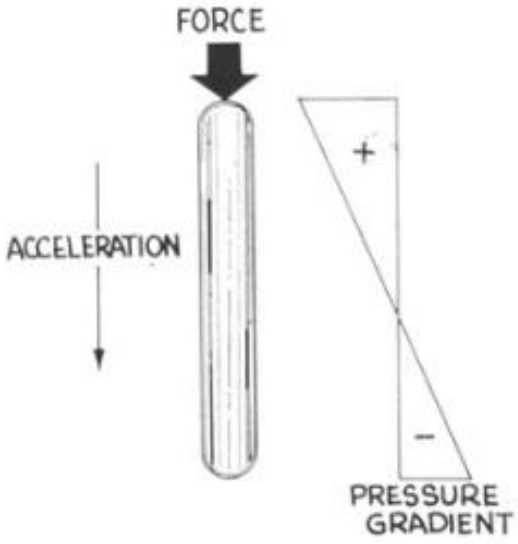

Figure. 1 Pressure gradient developed in a fluid-filled closed cuvette due to acceleration caused by an impact at one end [3]

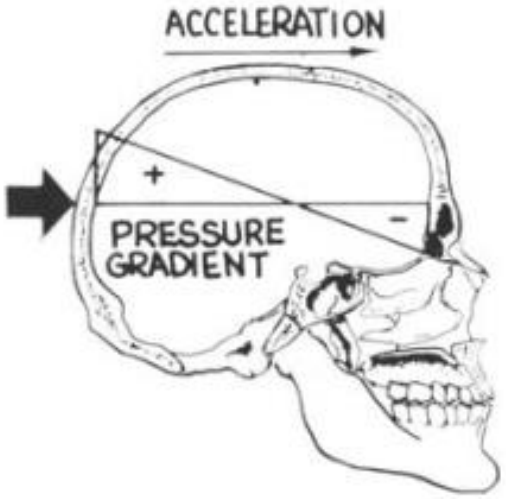

Figure. 2 Pressure gradient developed in the fluid of the brain due to acceleration caused by an impact to the head [3]

Several experimental studies have been carried out analyzing the linear or rotational acceleration of a head surrogate subject to blunt impacts but have neglected experimentally modeling the internal fluid to determine the pressure response in the coup and contrecoup regions [6] [7] [8] [9]. While this gives an understanding of the acceleration to post-incident patient conditions, it does not consider the internal brain mechanics. Efforts have been made using finite element modeling of realistic human head models with characterized human tissue

material properties, but they have lacked the experimental validation of the internal pressure developed within the brain [10] [12]. Both types of studies appear to lack a significant aspect of the macroscopic brain injury big picture. An integrated head impact study would ideally experimentally measure the impact conditions and internal material response while verifying the results with a one-to-one computational model. A study by Wardlaw and Goeller does just this. They design an experiment for the investigation of cavitation in water and Sylgard viscoelastic gel-filled ellipsoid surrogate model subject to variable shock tube blast conditions [13]. Pressure transducers were placed on the interior coup and contrecoup region to measure the time-dependent pressure response when subject to blast loading. This thesis' study takes a very similar approach to Ref [13] in the sense that the coup and contrecoup pressure of a fluid-filled ellipsoid shell subject to control loading will be analyzed via experiment and computational modeling. The main difference is that this study focuses on the blunt impact conditions and Ref [13] studies blast loading. Several computational and experimental studies confirm that the maximum pressure pulses at the time of impact occur in these localized coups and contrecoup regions.

The overall goal of this thesis is to correlate the impacting conditions of a fluid-filled surrogate human head model subject to a controlled impact to the intracranial pressure felt in the coup and contrecoup region. Two surrogate human head models were designed and 3D printed to simulate frontal and side head impacts. A simplified finite element model (FEM) was made using ANSYS Explicit Dynamics to simulate the pressure response developed in the coup and contrecoup subject to varying impact velocities. A dynamic pendulum impactor has been designed and manufactured in-house to deliver controlled impact conditions to the surrogate model. Intracranial pressure cannot be measured in-vivo, and thus a correlation to a measurable parameter such as acceleration may allow a link to tissue level damage.

CHAPTER 2

EXPERIMENTAL AND COMPUTATIONAL METHODS

This work is naturally collaborative with other researchers; Figure. 3 shows the multidisciplinary analysis that was conducted by different members of the group. In particular, major collaboration has taken place between Mr. Arthur Koster and me (Aaron Jackson). To clearly describe the scope of the overall project and identify individual contributions, the methods used to conduct the impact study are broken into two major categories: the physical experiment and computational modeling. Moreover, the experimental effort is broken into three categories including the test platform, the sensors, and the head surrogate. My (Aaron Jackson) contribution to the experimental setup includes the design and characterization of the pendulum impactor and the design and manufacturing of the head surrogate model. The entire computational study was done under the scope of this thesis as well.

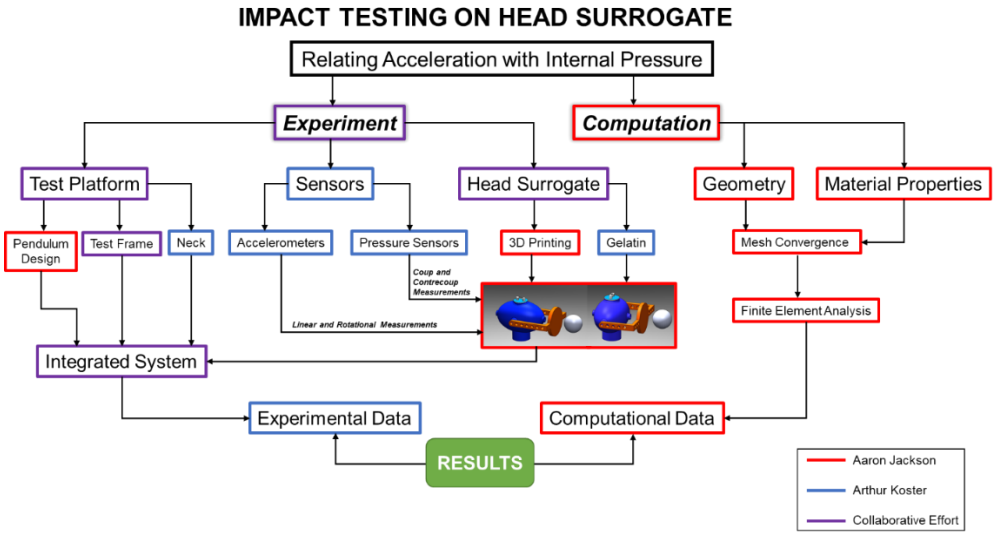

Figure. 3 Impact testing of a head surrogate model flow diagram with respective contributions

2.1 Experimental Setup

The objective of this study is to establish a correlation between impact conditions and the internal pressure response in the coup and contrecoup region of fluid-filled surrogate head

models. Both water and gelatin are used as the intracranial medium in the experiment. A unique experimental setup was designed as shown in Figure. 4. A pendulum impactor delivers a controlled input to the fluid-filled surrogate model.

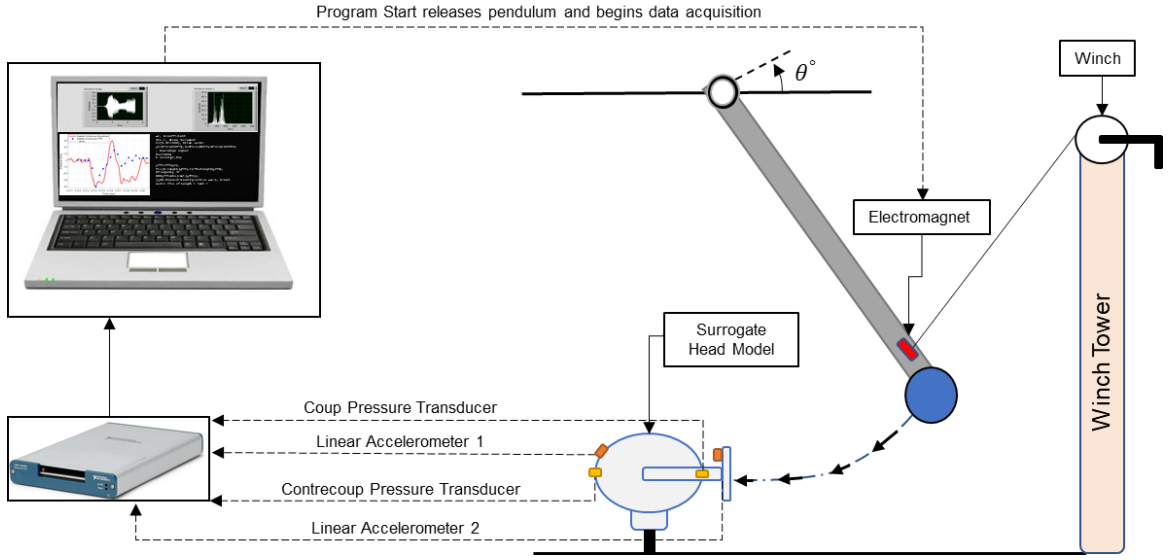

Figure. 4 Diagram of the experimental setup. A LabVIEW program is started which releases the pendulum arm via an electromagnet and begins data acquisition. Pressure transducers in the coup and contrecoup, and 2 linear accelerometers send data to NI DAQ which is saved on the computer for post-processing.

Two separate impact planes are considered in this study; the coronal model simulates a frontal impact, and the sagittal model simulates a side impact. Figure. 5 shows the CAD rendering of the coronal (frontal impact) plane model. The pressure sensor ports and accelerometer locations are indicated. Figure. 6 shows the CAD geometry of the sagittal (side impact) plane model. The ball that collides with an impact plate is also shown. The impacting plate was designed and incorporated into the head model design for two reasons. First, the impact plate protects the coup pressure sensor from damage when the impact occurs; without the impact plate, the sensor would be directly struck by the impactor and likely damaged. Second, the impact plate allows for the direct energy transfer to the head model midplane, or the location in which the impact arm is

attached to the head model. This essentially allows the head model and the impact plate to behave as a rigid body and thus experience the same bulk acceleration.

The average volume of the human brain has been recorded to be approximately between 1600 mL and 1200 mL for adults [14]. The internal volume of the shells was chosen to be 1212 mL. The ellipsoid major axis is 7 inches, and the minor axis is 5.5 inches. The shell thickness is 0.2 inches. Both models are the same geometry, the only difference is the orientation of the impact plate and the position of the pressure sensor ports.

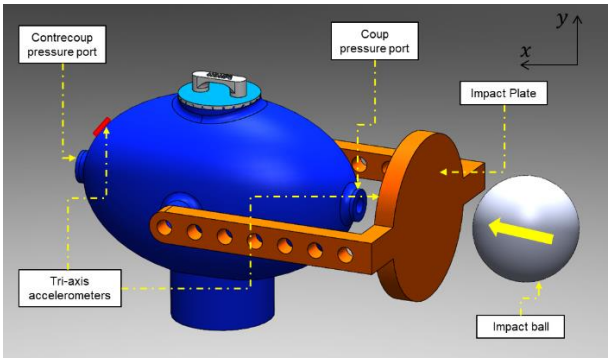

Figure. 5 Coronal plane surrogate model that simulates a frontal head impact

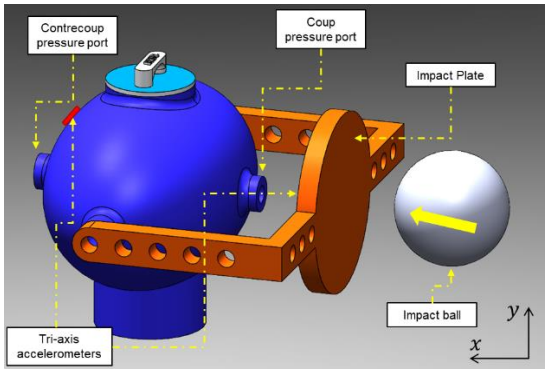

Figure. 6 Sagittal plane surrogate model that simulates a side head impact

The surrogate models were 3D printed using an HP Multi Jet Fusion 3D printer that uses the semi-crystalline polyamide, Nylon PA 12. The models were designed with holes in the coup and contrecoup for the installation of a Kulite XTEL190-S pressure transducer. Custom threaded pressure sensor inserts were manufactured to ensure the pressure sensor head is flush with the inside wall of the head model and there is a tight fit to mitigate any fluid leakage. The head models have two tri-axis accelerometers mounted for direct measurements of linear acceleration and the calculation of rotational acceleration. The scope of this study is limited to the response of the fluid-filled shell and thus a simplified “fixed” boundary condition neck model is used.

A digital angle measurement device is used to initialize the impacting pendulum to the desired drop angle. Each drop angle corresponds to a controlled impacting condition. The pendulum was engineered to deliver the desired range of impact parameters using a rigid body dynamics simulation. An electromagnet holds the pendulum arm and is attached to a rope which is fed into a winch that is cranked to set the desired pendulum angle. The electromagnet is powered by a function generator and synced with LabVIEW to trigger the release of the pendulum arm. When the LabVIEW program is started the electromagnet disconnects from the pendulum arm and begins 3 seconds of data collection at a sampling rate of 250,000 samples per second. The data is collected via a National Instruments Data Acquisition (DAQ) USB 6363. All data postprocessing is done via a MATLAB program. At each drop angle, three tests are performed to establish the standard deviation of the measured parameters. The experiment uses three types of internal fluid for each impact plane and at each impact velocity. Water is used as the baseline fluid which serves as a good start since it makes up approximately 77-78% of the human brain. The next two test sets of experiments use gelatin with a concentration roughly representative of white matter and gray matter mechanical properties.

2.2 Finite Element Modeling Methods

2.2.1 Finite Element Model Setup

Finite element analysis (FEA) was performed to simulate the impact event and resulting internal pressure response of the fluid-filled head model. ANSYS Explicit Dynamics was chosen for its capability to simulate impact events that happen on a small-time scale with highly transient pressure responses. Several head injury and automotive impact studies have utilized explicit solvers such as Explicit Dynamics and LS DYNA [15][16][17]. While explicit solvers typically come at a higher computational cost explicit analysis captures the small-time scale

transient responses in nonlinear materials. A symmetry model was utilized to cut down on computational time. The FEM coronal model is shown in Figure. *7* and the FEM sagittal model is shown in Figure. *8*.

The list of material properties used in the simulation can be found in Table I. A fixed boundary condition is applied to the head model base to simulate the rigid neck used in the experimental tests. The impacting ball is set as an initial velocity condition to impact the head model at the desired speed. The velocity of the impacting ball is parameterized to simulate all pendulum drop angle conditions from 20 to 80 degrees. The impact speeds of the pendulum impactor are determined analytically using rigid body dynamics and verified using high-speed digital image correlation (DIC). In the experimental model, the impact plate is rigidly bolted into the surrogate head to ensure that the arm and head act as a single rigid body. Therefore, the contact between the impact arm and head model is defined as a bonded contact. The internal fluid is defined as a bonded contact to the interior of the ellipsoid shell.

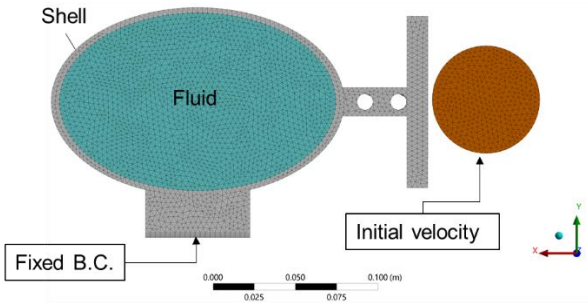

Figure. 7 Finite element model of the coronal plane fluid-filled ellipsoid with specified boundary conditions

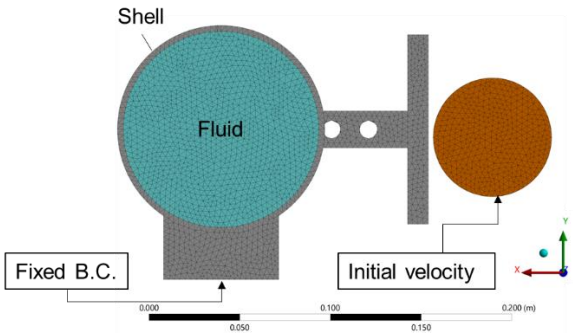

Figure. 8 Finite element model of the sagittal plane fluid-filled ellipsoid with specified boundary conditions

The internal pressure developed in the coup and contrecoup was calculated using the average hydrostatic fluid stress across 3 elements in the region of interest. Each fluid element is subject to both normal and shear stress and can be described by the stress tensor:

$$\sigma_{ij} = \begin{bmatrix} \sigma_{xx} & \tau_{xy} & \tau_{xz} \\ \tau_{yx} & \sigma_{yy} & \tau_{yz} \\ \tau_{zx} & \tau_{zy} & \sigma_{zz} \end{bmatrix} = \sigma' + \sigma_{Hyd} \quad (1)$$

where σ' is the deviatoric stress and σ_{Hyd} is the hydrostatic stress. The deviatoric stress carries all the information regarding shear and the hydrostatic stress carries the information of the normal stress. The hydrostatic stress can be expressed as the average of the three normal stress components.

$$\sigma_{Hyd} = \frac{1}{3}(\sigma_{xx} + \sigma_{yy} + \sigma_{zz}) \quad (2)$$

The pressure is then simply just the negative of the hydrostatic stress.

$$P = -\sigma_{Hyd} = -\frac{1}{3}(\sigma_{xx} + \sigma_{yy} + \sigma_{zz}) \quad (3)$$

For each simulation, the hydrostatic stress and pressure are calculated in the fluid region of interest. The average stress over three element faces are taken to be the pressure in the coup and contrecoup region; these are the pressure values that are later compared to the experimental results. Experimental results indicated the highly transient portion of the pressure event occurred in under 10 milliseconds; therefore, the simulation run time was chosen to be 10ms.

2.2.2 Mesh Convergence Study

To gain confidence in the chosen mesh size, a mesh convergence study was performed for both the coronal and sagittal plane models. For element sizes ranging from 14 mm to 3 mm, a simulation for the 80-degree impact condition was performed. Figure. 9 and Figure. 10 shows the maximum pressure developed in the coup and contrecoup region for the coronal and sagittal models, respectively. As the element count was increased the recorded pressure in the regions of interest was tracked until convergence was assumed within an acceptable tolerance of 5%. For the coronal model, the mesh was assumed to converge at an element size of 3 mm. For the

sagittal model, the mesh size was assumed to have converged for an element size of 4 mm. The simulation time for the coronal model took 63 minutes. The time for one sagittal simulation to complete was 28 minutes. The approximate times that each simulation took for the respective element size are included in Figure. 9 and Figure. 10.

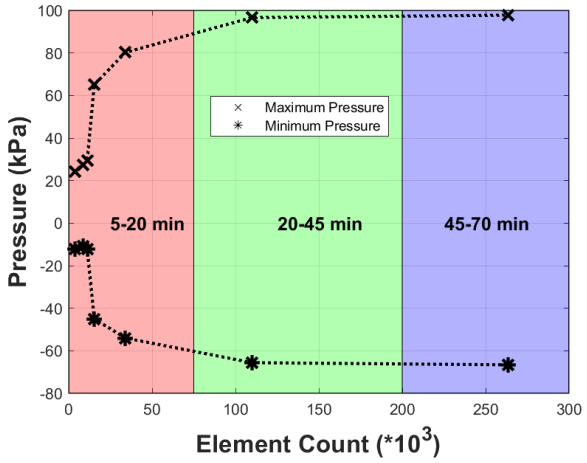

Figure. 9 Coronal model mesh convergence study (all simulations run with 14 cores at an impact velocity of 5.5m/s)

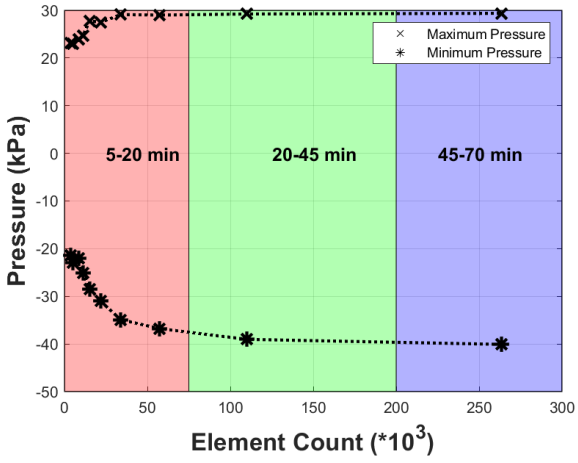

Figure. 10 Sagittal model mesh convergence study (all simulations run with 14 cores at an impact velocity of 5.5m/s)

Table I Head Model Material Properties

	Density $[kg/m^3]$	**Young's Modulus** **[Pa]**	**Poisson's Ratio** **[-]**	**Bulk Modulus** **[Pa]**
PA Nylon 12	1001	1800E06	0.35	--
Ninja-flex	1018	12E06	0.45	--
Water	998.2	--	---	2.15E09

2.3 Characterization of Dynamic Test Platform

The characterization of the impacting test platform is important to correlate the impact conditions to the internal pressure. It is also important for the proper representation of the initial conditions for the FEM model. Using rigid body dynamics, the mass and inertia properties for both the pendulum arm and the impact ball can be considered and included in the formulation of the equation of motion. Solving the equation of motion for the acceleration and velocity at the position of the impact ball will give all necessary input parameters for the study. Figure. 11 gives a schematic of the test platform containing the two rigid bodies.

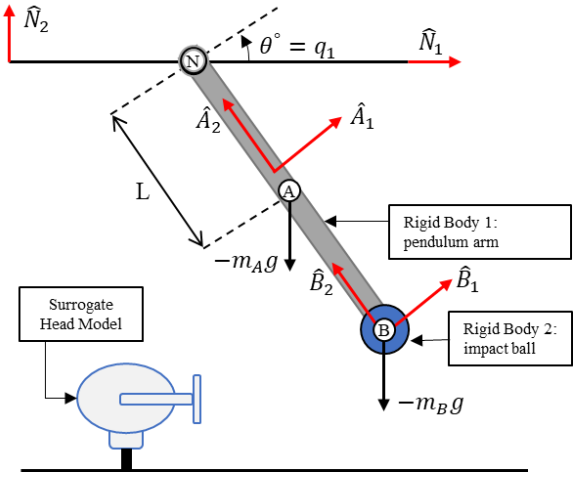

Figure. 11 Schematic of impact pendulum with the corresponding body frames, forces, and dimensions

Point N is the inertial point and frame N is the inertial frame. This frame and point are non-accelerating and are analogous to the lab frame. Rigid body A is the pendulum arm and has a center of gravity at point A. Frame A is rigidly rotating with body A. Rigid body B is the impact ball and carries its own inertia and mass. Point B is the impact ball center of gravity and frame B rigidly rotates with body B. In this instance, body A and B are dependent because they are rigidly connected; therefore, the rotation matrix at any given point for body A is equivalent to the rotation matrix of body B. The pendulum is initialized at an angle q_1 which is the only

generalized coordinate. There are no constraints on the system therefore there is only one degree of freedom. Gravity forces act at the center of gravity of each body. The relationship between the body attached frames and the inertial frame are given by the rotation matrices for bodies A and B, where R_A^N is the transformation matrix from frame N to A and R_B^N is the transformation matrix from frame N to B.

$$R_A^N = R_B^N = \begin{bmatrix} \cos(q_1) & -\sin(q_1) & 0 \\ \sin(q_1) & \cos(q_1) & 0 \\ 0 & 0 & 1 \end{bmatrix} \tag{4}$$

First, the position vectors from inertial point N to each body can be defined.

$$\vec{P}_{NA} = -L\hat{A}_2 \tag{5}$$

$$\vec{P}_{NB} = -2L\hat{A}_2 \tag{6}$$

The position vectors can be differentiated using the transport theorem to obtain the linear velocity.

$$\vec{V}_{NA} = L\dot{q}_1\hat{A}_1 \tag{7}$$

$$\vec{V}_{NB} = 2L\dot{q}_1\hat{A}_1 \tag{8}$$

The angular velocity can be inferred by observation. Both bodies are rotating about the $\widehat{N}_3$ axis by an angle q_1. Since frames A and B are equivalent the angular velocities are also the same and given by Equation (9).

$$\omega_{NA} = \omega_{NB} = \dot{q}_1 \hat{A}_3 = \dot{q}_1 \hat{N}_3 \tag{9}$$

The linear acceleration of points A and B is found by differentiating the velocity vectors using the transport theorem.

$$\vec{A}_{NA} = L\ddot{q}_1 \hat{A}_1 + L\dot{q}_1^2 \hat{A}_2 \tag{10}$$

$$\vec{A}_{NB} = 2L\ddot{q}_1 \hat{A}_1 + 2L\dot{q}_1^2 \hat{A}_2 \tag{11}$$

Half the length of the pendulum arm is $L = 0.4572\ m$. Body A has a mass of 2.4 kg and an inertia $I_{xx_A} = 0, I_{yy_A} = 0$, and $I_{zz_A} = 0.49\ kgm^2$. Body B has a mass of 0.22 kg and an inertia of $I_{xx_B} = 0, I_{yy_B} = 0$, and $I_{zz_B} = 1.2E-4\ \ kgm^2$. The only forces acting on the system are gravity for both bodies. There are no moments applied to the system. The generalized active forces and inertia forces are given by Equations (12) and (13), respectively. Kane's method is given by Equation (14) and is developed from Euler's First and Second Laws with consideration of the total work done on the system [18].

$$F_i = \sum_{K}^{bodies} (\Sigma F)_K \cdot \frac{\partial V_K}{\partial\ \dot{q}_\iota} + (\Sigma M)_K \cdot \frac{\partial \omega_{NK}}{\partial \dot{q}_i} \tag{12}$$

$$F_i^* = \sum_{K}^{bodies} m_K \dot{V}_K \cdot \frac{\partial V_K}{\partial \dot{q}_i} + \frac{dH_{KK}}{dt} \cdot \frac{\partial \omega_{NK}}{\partial \dot{q}_i} \tag{13}$$

$$F_i - F_i^* = 0 \tag{14}$$

Using Equations (7) - (13), the equation of motion for the system shown in Equation (15) is found.

$$-2gLm_B \sin(q_1) - gLm_A \sin(q_1) - \left(I_{ZZ_A} + I_{zz_B} + m_A L^2 + 4m_B L^2\right)\ddot{q}_1 = 0 \qquad (15)$$

A rigid body dynamics simulation software called Autolev was used to solve the equation of motion for the position, velocity, and acceleration of body B for initial conditions $q_1 = 20^\circ$ to $q_1 = 80^\circ$ in increments of 10°. The acceleration and velocity of the impact ball were calculated at the moment of impact when $q_1 = 0^\circ$. Figure. 12 and Figure. 13 show the change of velocity and acceleration with angle position for an initial condition $q_1 = 45^\circ$.

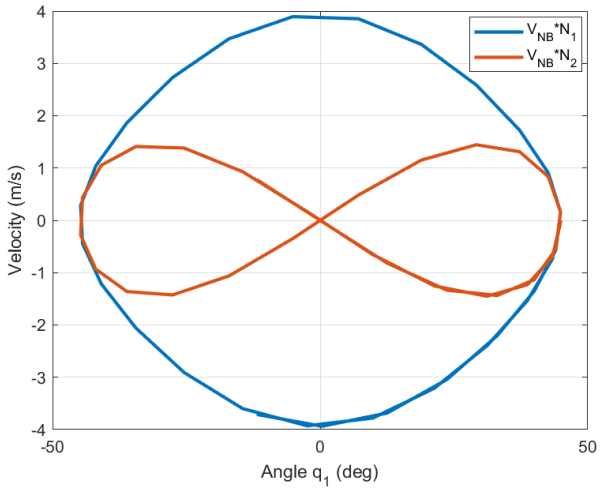

Figure. 12 Pendulum velocity with angle position for an initial release at $q_1 = 45^\circ$. The horizontal velocity is maximum at impact and the vertical velocity is zero.

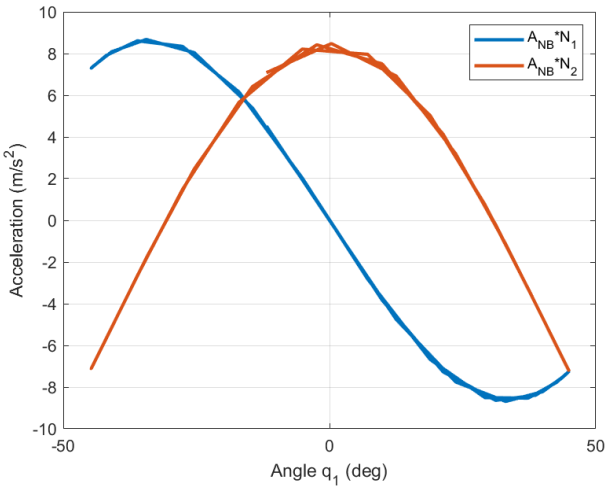

Figure. 13 Pendulum acceleration with angle position for an initial release at $q_1 = 45^\circ$. The horizontal acceleration is zero at impact and the vertical acceleration is maximum.

The maximum horizontal velocity in the $\hat{N}_1$ direction occurs at impact when the vertical velocity in the $\hat{N}_2$ direction is zero. The horizontal acceleration in the $\hat{N}_1$ direction is zero at impact and the vertical acceleration is maximum.

To verify the dynamic simulation a Photron FASTCAM high-speed camera was used to perform digital image correlation (DIC) on the impact ball. For each system initial condition, a

high-speed video was taken of the impact ball at the moment of impact ($q_1 = 0^{\circ}$). Photron's FASTCAM Viewer (PFV) software allows for an easy DIC analysis by tracking the displacement of objects of interest between frames. The results of the rigid body dynamics simulation and the high-speed camera DIC analysis are shown in Figure. 14 [19].

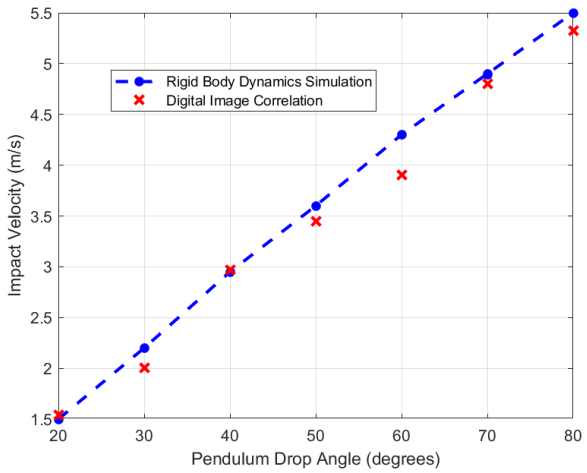

Figure. 14 Comparison of predicted impact velocity for pendulum initial conditions 20-80 degrees for the rigid body dynamics analytical simulation model and using digital image correlation

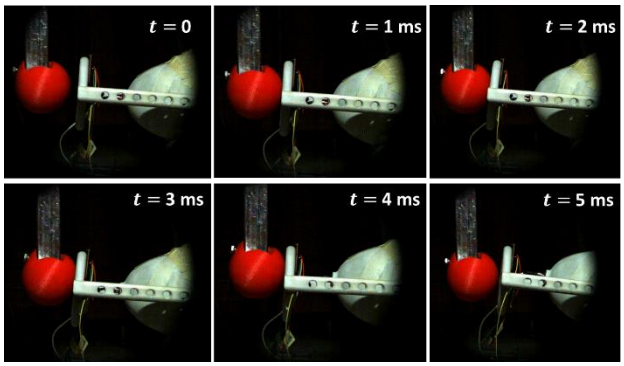

Figure. 15 Frames taken from the high-speed camera footage for an 80-degree impact of the coronal model. DIC was performed on the impact ball for the time preceding the collision.

The rigid body dynamic simulation and the DIC agree well with one another. At drop angels of 20°, 40°, 70°, and 80°, the calculated velocity is within 4% of the observed value. The largest difference is at a drop angle of 60° where the calculated value is within 9% of the observed value. Discrepancies in the impact velocity can be attributed to errors associated with the digital angle measure device.

2.4 Theoretical Modeling of Impacting Fluid-filled Shells

In 1998 P.G. Young and C. L. Morfey explored the intracranial pressure transients developed in a fluid-filled shell subject to a blunt impact by finite element modeling [20]. They found that the transient pressure response developed in the pole and antipole regions could be predicted by

using the ratio of the period of oscillation T_Ω of the first n=2 spherical mode of vibration of a fully free shell and the impact duration T_p [20]. "An approximate closed-form expression that accurately predicts the period of oscillation T_Ω was derived based on the exact solution for a membrane filled with incompressible fluid for the spherical shell case", [21]. The closed-form approximation for the oscillatory period is given by Equation (16).

$$T_\Omega = \sqrt{\frac{3\pi(5+\upsilon_{sh})m_{sh}}{8hE_{sh}}} \tag{16}$$

υ_{sh} is the Poisson's ratio of the shell, m_{sh} is the mass of the shell, E_{sh} is the Young's modulus of the shell, and h is the thickness of the shell. For this study, the shell thickness is 0.2 inches, and the mass is 0.467 kg. Other properties for the shell can be found in

Table I. Ref. [20] showed that for $T_p/T_\Omega > 4$ the pressure response was considered hydrostatic which gives a linear pressure gradient from the positive coup to the negative contrecoup region. Ref [21] presents the hydrostatic pressure as Equation (17).

$$P_{quasi} = \frac{F_{max}\rho_f R_f}{m_{sh}} \tag{17}$$

F_{max} is the maximum impact force delivered to the fluid-filled shell. This is essentially the measured acceleration of the impacted surrogate head model multiplied by the mass. ρ_f is the fluid density, R_f is the radius of the fluid, and m_{sh} is the mass of the shell. Since this analysis considers an ellipsoid and not a spherical shell, R_f is assumed to be the fluid radius in the direction of impact. It is assumed for the coronal model $R_f = .084\,m$ and the sagittal model $R_f = .05\,m$. Figure. 16 shows a diagram of the coronal model representing the key parameters for the aforementioned analytical model.

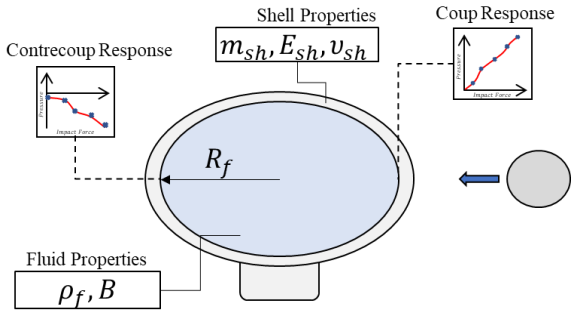

Figure. 16 Diagram representing the impact model with shell and fluid properties labeled.

It was shown that for ratios of impact time to the oscillatory time less than 4, dynamics pressure responses occurred with large pressure peaks. Their simulation applied a Hanning force-time history over the shell membrane which was argued to be an accurate impact model because an impact lies between a half-sine and a half-sine to the 3/2 power forcing function [21]. The maximum pressure developed in the coup and contrecoup region is approximately given by Equation (18). This equation was obtained using results from Ref. [20].

$$P_{max} = 32P_{quasi}e^{-2\left(\frac{T_p}{T_\Omega}\right)} = \frac{32F_{max}\rho_f R_f e^{-2\left(\frac{T_p}{T_\Omega}\right)}}{m_{sh}} \tag{18}$$

For the conditions $\frac{h}{R_f} < 0.4$ and $\left(\frac{Eh}{BR_f}\right) < 1$, the maximum error using Equation (16) was reported as being less than 10% when compared with using full three-dimensional elasticity equations [21]. Both conditions are met for the coronal and sagittal plane models used in this study. These simulations were performed using a free boundary condition. It's been stated by previous works that for impact durations less than 6 ms, the neck restraint boundary condition is unlikely to affect the head response [10] [22]. Therefore, other than the effects of using an ellipsoidal shell rather than a spherical, the model should serve as a reasonable first-order prediction. Figure. 17 shows a range of predicted pressures in pole for F_{max} values ranging from 10 N to 2000 N for

the coronal plane model. Figure. 18 shows the predicted pressure values in the pole for the sagittal plane model with F_{max} values ranging from 10 N to 2000 N. Both figures used impact times of 2 ms.

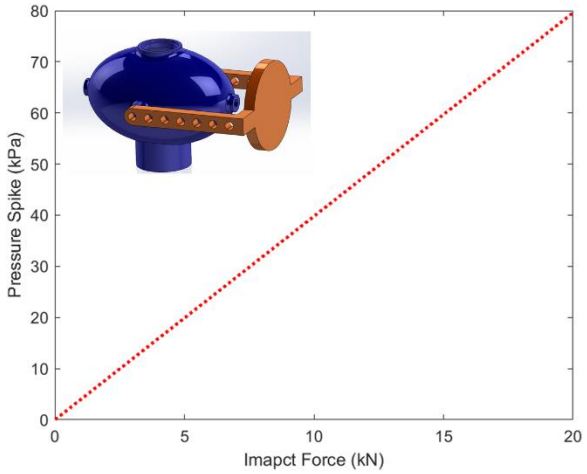

Figure. 17 Analytical model for the maximum pressure at the pole of an impacted fluid-filled shell with fluid radius assumed along the ellipsoid major axis

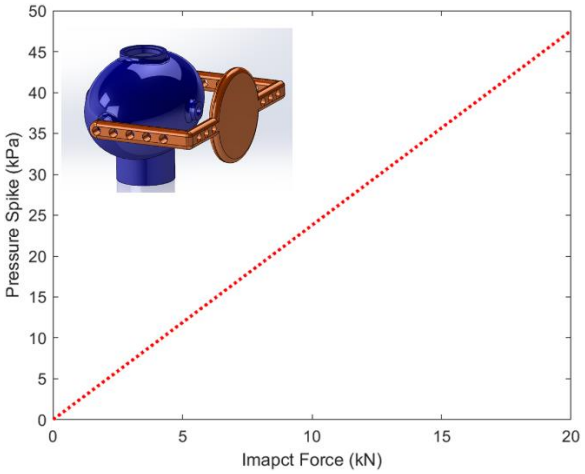

Figure. 18 Analytical model for the maximum pressure at the pole of an impacted fluid-filled spherical shell with fluid radius assumed equal to the sagittal ellipsoid minor axis

CHAPTER 3

RESULTS

3.1 Coronal Plane Water

The coronal model converged at an element size of 3mm with 263,330 total elements. The variation of pressure developed in the coup and contrecoup with varying impact velocity is shown in Figure. 19. The experimental results presented are the mean value over 3 tests for each drop angle [19]. Overall, the coronal FEM had a better agreement with the experiment for the coup region. Although, the FEM coup region underpredicted the compressive pressure response for all angles except at the maximum impact velocity where it just barely overpredicted the response. In the contrecoup region, the FEM pressure underpredicted the magnitude of the experimental tensile pressure from velocities 1.5m/s to 3.6 m/s. From impact velocities 3.6 m/s to 5.5 m/s the FEM model overpredicted the magnitude of the tensile pressure. The P.G. Young analytical model showed an agreeable trend to both the FEM and experiment. The analytical model overpredicted the magnitude of tensile pressure formed in the contrecoup region. It also underpredicted the magnitude of compressive pressure formed in the coup. Since the analytical model was derived for spherical geometry, it makes sense that the pressure development would have slight discrepancies. It was also performed using a free boundary condition. However, it's been stated by previous work that for impact durations less than 6 ms, the neck restraint boundary condition is unlikely to affect the head response [10] [22]. The comparison of these models may be an indication that this is true.

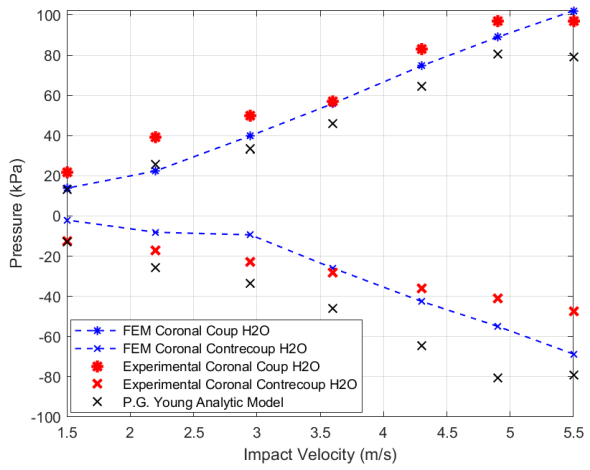

Figure. 19 Coronal FEM and experimental result comparison for the pressure developed in the coup and contrecoup region for varying impact velocity

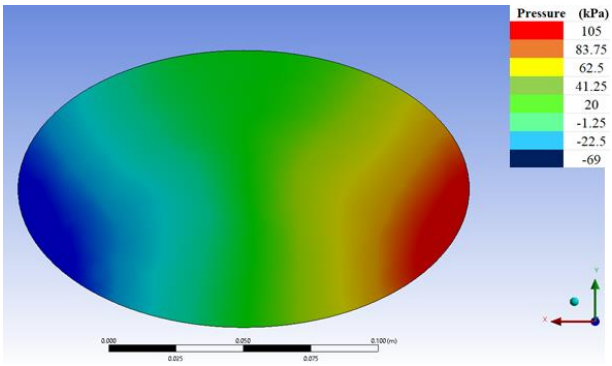

Figure. 20 Pressure response of coronal plane surrogate model with an impact velocity of 5.5 m/s at the peak impact time.

Figure. 20 shows the pressure gradient developed in the fluid at the peak pressure response time of 2.6ms. Maximum compressive pressure of 102 kPa was formed in the coup. Maximum tensile pressure of -68 kPa was formed in the contrecoup. The maximum pressure developed was not recorded in the coup and contrecoup region, but the region about 10 mm below. In the coronal simulation, the maximum pressure developed was 105 kPa in the coup and -69 kPa in the contrecoup. It is therefore possible that the location of maximum compressive and tensile pressure was not captured in the experiment sensor location. Based on the FE model higher magnitude pressures could have been developed just beneath the coup and contrecoup sensor location. An accepted tensile pressure to assume cavitation has occurred is approximately -100 kPa in water [13] [12]. This level of negative pressure was not achieved in the coronal FEM simulation nor the experimental results at the maximum impact condition. Additional simulations for this model indicate that an impact velocity of approximately 10 m/s would be needed for the FEM model to achieve a contrecoup tensile pressure of -100 kPa. Figure. 21 shows a time-dependent response of the pressure in the coup region compared to an experimental test with the

same impact conditions of 5.5 m/s. Figure. 22 shows the time-dependent behavior of the contrecoup for the impact velocity of 5.5 m/s.

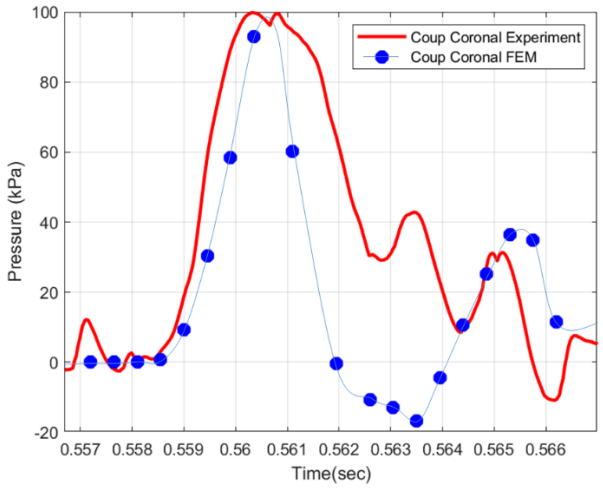

Figure. 21 Comparison of time-dependent behavior of the coronal FEM model and experimental results in the coup region

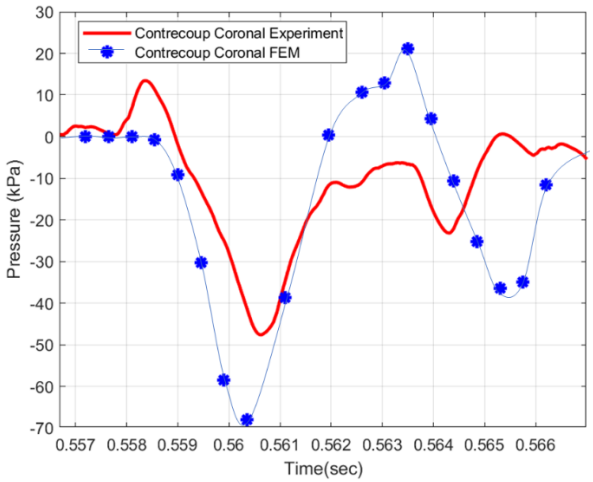

Figure. 22 Comparison of the time-dependent behavior of the coronal FEM model and experimental results in the contrecoup region

Figure. 21 shows a very favorable agreement between the FEM simulation and the experiment up to the peak pressure. The simulation predicted a shorter total impact time as the curve is seen to peak over a shorter time compared to the experiment. The simulation predicted an approximate 2ms impact time while the experiment indicated an impact time of 2.5 ms. The experiment showed oscillation of the pressure as it decreased from the peak value and returned to steady-state. The FEM simulation showed more of an ideal sinusoidal damped motion as compared to the coup experimental results. In the contrecoup region, the experiment also showed oscillatory fluctuations as it reduced from the peak pressure back to steady-state. The simulation showed a smooth sinusoidal damped motion as it moves from peak tensile pressure to a lower magnitude compressive pressure before returning steady state.

Several head injury studies have focused on the effects of skull deformation via strain gauge measurements in experiments or by varying the elasticity of the skull material to

understand its correlation to the internal pressure developed in the surrogate models [20] [13]. Ref. [20] concluded that varying the Poisson's ratio of the skull material only had a small effect on the pressure response developed in the fluid. It was also found that the flexibility of the skull material has much more of an effect on the pressure response than the bulk modulus of the internal fluid. Other blast-induced surrogate studies show that deformation of the shell or skull is a major factor that contributes to fluids pressure gradient formation and in some cases of extreme tensile pressure development results in cavitation [13] [23]. Figure. 23 shows the deformation developed in the FEM model for an impact velocity of 5.5 m/s.

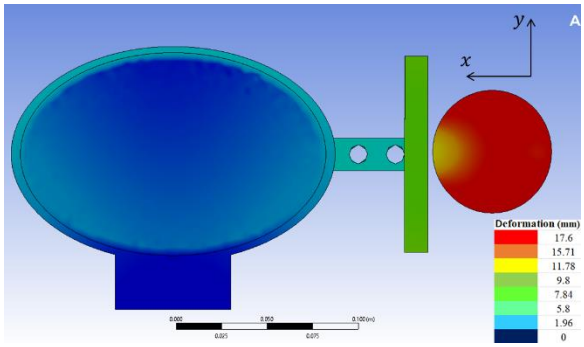

Figure. 23 Deformation of water filled ellipsoid subject to impact from a ball traveling at a velocity of 5.5 m/s.

The maximum recorded deformation occurred in the impacting ball which is of no surprise since the material properties of 3D printed Ninjaflex yield a highly deformable material. The largest deformations on the ellipsoid shell occur on the upper shell surface with a deformation of about 5.19 mm. The deformation of the ellipsoid shell on the exterior of the coup and contrecoup regions is approximately 1.98 mm and 1.74mm, respectively. This deformation correlates to a pressure of 102 kPa and -68 kPa in the coup and contrecoup at peak impact time. The impact plate experienced the highest deformation other than the impact ball with a displacement of around 9.8 mm.

3.3 Sagittal Plane Water

The sagittal FEM model converged at an element size of 4mm with 109,960 total elements. The variation of coup and contrecoup pressure developed over varying impact velocity is seen in Figure. 24 for the experimental results, FEM simulation, and the P.G. Young analytical model. The experimental results presented are the mean value over 3 tests for each drop angle. The coup experimental results show a shallow linear trend increasing from roughly 10kPa to 23 kPa. The contrecoup experimental results show a non-linear trend ranging from roughly -15 kPa to -38 kPa. The FEM coup predicted a steeper curve and a larger range than the experiment. The maximum FEM coup pressure at 5.5 m/s impact velocity is 34 kPa while the experiment showed 23 kPa yielding the largest difference of 38.5%. At other impact velocities, the comparison was nearly identical. For a drop angle of 30 and 40 degrees, the coup and contrecoup experimental measurements were within 5% of those predicted by the FEM simulation and the analytical model. The contrecoup experimental measurements did not show an entirely linear trend. In the range of 2.95 m/s to 4.3 m/s the tensile pressure decreased before rapidly increasing between 4.3 m/s and 5.5 m/s. The experimental contrecoup pressure at the maximum impact velocity is -37.36 kPa while the FEM model is -40.9 kPa. The analytical model maximum tensile pressure was found to be -40.76 kPa. This yields an 8% difference from the experiment and a 0.34% difference from the finite element model. The maximum compressive and tensile pressure formed in the sagittal model was not developed in the measured coup and contrecoup region but about 8 mm below. The maximum compressive pressure developed at the peak impact time was 36.1 kPa and the maximum tensile pressure was -41.8 kPa.

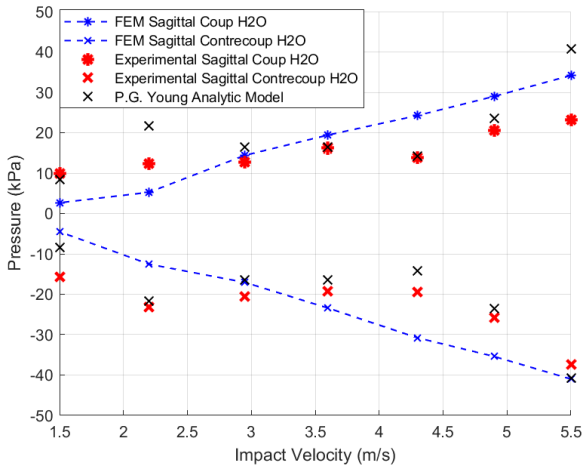

Figure. 24 Sagittal FEM and experimental results comparison for the pressure developed in the coup and contrecoup region for varying impact velocity

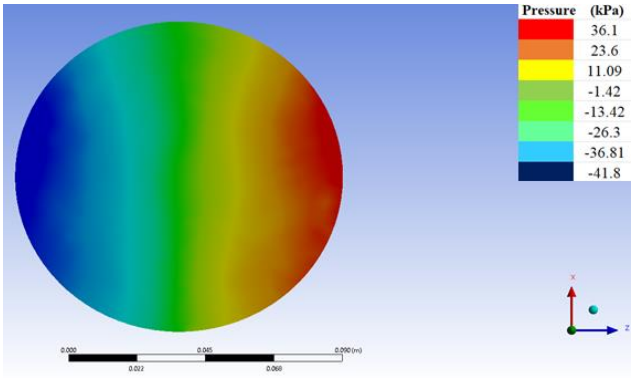

Figure. 25 Pressure gradient of the sagittal plane surrogate model with an impact velocity of 5.5m/s at the peak impact time

The deformation produced in the sagittal plane model showed to be very similar but slightly higher to that of the coronal model. Figure. 26 shows the total deformation for a sagittal FEM simulation with an impact velocity of 5.5 m/s. The maximum deformation on the shell developed on the upper exterior surface with a displacement of 5.97 mm. The deformation in the coup and contrecoup region on the shell surface was recorded to be 1.99 mm and 1.84 mm, respectively. These deformations correlate to pressures of 34 kPa and -40.9 kPa in the coup and contrecoup region, respectively.

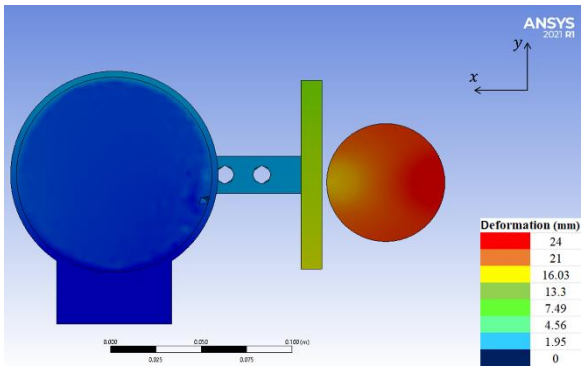

Figure. 26 Deformation of sagittal plane FEM simulation subject to an impact velocity of 5.5 m/s.

The time-dependent response for an impact at 80 degrees in the sagittal model is shown in Figure. 27 and Figure. 28. Figure. 27 shows the response of the sagittal plane coup region for both the experimental and FEM data. Figure. 28 shows the response of the sagittal plane contrecoup region for both the experimental and FEM data.

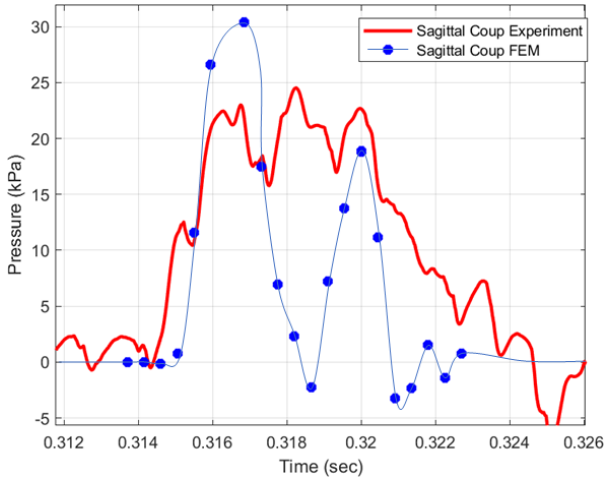

Figure. 27 Coup response in the sagittal plane model subject to an impact velocity of 5.5 m/s

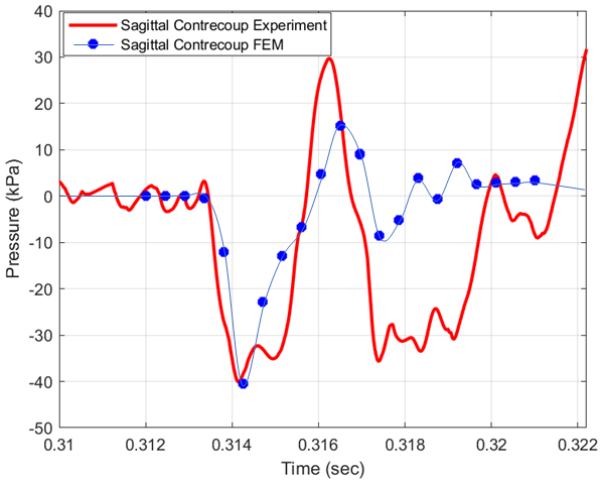

Figure. 28 Contrecoup response of the sagittal plane model subject to an impact velocity of 5.5 m/s

The experimental data shown in Figure. 27 shows an oscillatory fluctuation after impact where the FEM model predicted a more standard second-order system decaying response. In the coup region, the impact at eighty degrees was overpredicted by the FEM model by nearly 11 kPa. In the contrecoup region, the tensile pressure was nearly exact when compared to the experimental data. The impact time of the FEM sagittal model at eighty degrees was 2.5 ms – 3 ms. The experimental data shows an impact time of roughly 3 ms -4 ms for the coup and 2 ms-2.5 ms for the contrecoup.

3.4 Conclusion

This study designed, manufactured, and characterized a pendulum impactor for the delivery of controlled loading to fluid-filled surrogate human head models. Two realistically

sized 3D printed head models were studied for the frontal and side impact planes. A range of experiments for water and gelatin-filled head models were performed for varying impact velocities ranging from 1.5 m/s to 5.5 m/s which were led by [19]. Experimental pressure data was recorded in the coup and contrecoup regions for both fluid mediums. A finite element model was designed utilizing ANSYS Explicit Dynamics for the determination of the internal water pressure responses subject to variable velocity impact conditions. An analytic model to predict the internal pressure spikes in the pole and anti-pole regions for a fluid-filled spherical shell (P.G. Young 2002) was used as a simplified theoretical model for comparison to results.

3.4.1 Coronal Water model results

In the coup region, the experimental results showed a higher-pressure response than the FEM and analytic model except for the maximum impact velocity of 5.5 m/s. At an impact of 5.5 m/s, maximum compressive pressure of 97 kPa was recorded in the experiment, 102.1 kPa in the FEM model, and 79 kPa in the analytic model. At the maximum impact velocity, the FEM and experiment coup pressure were within 5.3% of each other, while the analytic model and the experiment were within 18.5% of each other. The maximum tensile pressure recorded in the contrecoup during the experiment was -47.3 kPa. The maximum tensile pressure in the contrecoup predicted by the FE model was -68 kPa, yielding an error of nearly 30%. The analytic model overpredicted the tensile pressure formation even more at -79 kPa. At 3.6 m/s impact velocity, the agreement between the FE model and the experimental results are nearly identical with an error of less than 5%. The time-dependent behavior of the 80-degree impact shows that the FE model predicts a shorter impact time in the coup than the experiment, while the contrecoup shows very similar transient behavior. The impact time for the coronal water models is roughly 2-3 ms. The maximum recorded deformation of the ellipsoid shell in the coup and

contrecoup region is 1.98 mm and 1.74 mm, respectively. This deformation correlates to pressures of 102 kPa and -68 kPa.

3.4.2 Sagittal Water model results:

In the coup region, the sagittal FE model under-predicted the compressive pressure formed for the first two drop angles and over-predicted the pressure in the remaining higher drop angles. The maximum coup compressive pressure developed for impact speeds of 5.5 m/s were 23 kPa in the experiment and 34 kPa in the FE model, yielding a difference of about 32%. At impact speeds of 2.95 m/s the experiment and FE model match more closely in the coup and contrecoup with an error of less than 15%. At this speed, the coup recorded a pressure of 12.65 kPa and 14.4 kPa for the experiment and FE model, respectively. Similarly at this speed, the contrecoup recorded a pressure of -20.64 kPa and -23.42 kPa for the experiment and FE model, respectively. The analytic model showed a similar trend to the experimental results since the peak force transmitted was calculated based on the measured acceleration. In the contrecoup, the analytical model predicted exceedingly well for nearly all impact speeds. In the coup, the analytical model predicted best between speeds of 2.95 m/s to 4.95 m/s. The experimental time response of the coup pressure sensor yields a fluctuation at high pressures following the peak pressure event; this fluctuation is not seen in the FE model. The experimental time response of the contrecoup region for an impact velocity of 5.5 m/s shows very agreeable behavior of the initial negative pressure spike, however, the following compressive pressure formation recorded in the experiment is of higher magnitude than that predicted by the model. The time response for the sagittal plane model showed roughly 3-4ms in the coup and 2-2.5 ms in the contrecoup. The maximum recorded deformation of the ellipsoid shell at a 5.5 m/s impact was 1.99 mm and 1.84

mm in the coup and contrecoup, respectively. This correlated to pressures of 34 kPa and -40.9 kPa in the coup and contrecoup.

3.4.3 Comparison

In comparison, the pressures developed in the coronal model were higher than those developed in the sagittal model. This was consistent between the experimental results, the FE model, and the analytical model. For the same impact conditions, the FE model showed the maximum coup pressure developed in the sagittal model to be 33% of that developed in the coronal. The experiment showed the sagittal coup to be 24% of the coronal coup pressure. The FE model also showed the sagittal contrecoup pressure was 58% of that developed in the coronal model, while the experiment showed the sagittal contrecoup to be 78% of the coronal model. Both the experiment and FEM show the coronal plane exhibits larger pressure magnitudes in the coup region with a lesser magnitude in the contrecoup. Opposite to this, the experiment and FEM agree that the sagittal plane exhibits larger pressure magnitudes in the contrecoup region when compared to the coup region. Discrepancies in the FEM and experimental model can be attributed to a few aspects of this study. The experimental head model was fixed as rigidly as possible to the test stand base plate, however, high-speed camera footage verifies that there is still a small amount of movement when subject to an impact as the FEM used an ideal “fixed” boundary condition this results in a non-1-1 match between the experiment and modeling technique. Future works will focus more on verifying the boundary conditions are as similar as possible to avoid modeling discrepancies. Additionally, material properties for the 3D printed materials were taken from sources. The specific materials used in this experiment are slightly different than those reported by the manufacturer. In future works, material testing will be

prioritized to ensure the exact material properties of the system are being considered in the model.

Acknowledgment
This work has been funded by the Office of Naval Research (ONR) (Award #N00014-18-1-2082 – and N0014-21-1-2051. Dr. Timothy Bentley, Program Manager).

References

[1] M. James P. Kelly, "Traumatic Brain Injury and Concussion in Sports," *JAMA*, pp. 989–991, 1999.

[2] K. Brolin, "Correlation of global head and brain tissue injury criteria to experimental concussion derived from monkey head trauma experiments," 2013. [Online]. Available: https://www.researchgate.net/publication/287756456

[3] A. G. Gross, "A NEW THEORY ON THE DYNAMICS OF BRAIN CONCUSSION AND BRAIN INJURY*."

[4] W. Kang, A. Ashfaq, T. O'shaughnessy, and A. Bagchi, "Cavitation Nucleation in Gelatin: Experiment and Mechanism," 2017.

[5] Z. Pan *et al.*, "Cavitation onset caused by acceleration," *Proceedings of the National Academy of Sciences of the United States of America*, vol. 114, no. 32, pp. 8470–8474, Aug. 2017, doi: 10.1073/pnas.1702502114.

[6] A. King, K. Yang, and L. Zhang, "Is Head Injury Caused by Linear or Angular Acceleration? Injury predictors for traumatic axonal injury in a rodent head impact acceleration model View project Projects in impact biomechanics View project," 2003. [Online]. Available: https://www.researchgate.net/publication/242211067

[7] B. Thorne, "Pendulum Based Impact Testing of Athletic Helmets Using the NOCSAE Headform," 2016. [Online]. Available: https://digitalscholarship.unlv.edu/thesesdissertations/2907

[8] A. Singh, S. G. Ganpule, M. K. Khan, and M. A. Iqbal, "Measurement of brain simulant strains in head surrogate under impact loading," *Biomechanics and Modeling in Mechanobiology*, vol. 20, no. 6, pp. 2319–2334, Dec. 2021, doi: 10.1007/s10237-021-01509-6.

[9] L. Zhang, K. H. Yang, and A. I. King, "A Proposed Injury Threshold for Mild Traumatic Brain Injury," *Journal of Biomechanical Engineering*, vol. 126, no. 2, pp. 226–236, Apr. 2004, doi: 10.1115/1.1691446.

[10] M. D. Gilchrist, “The creation of three-dimensional finite element models for simulating head impact biomechanics,” 2003.

[11] A. Eslaminejad, M. Hosseini-Farid, and M. Ziejewski, *Comparative Study of Coup and Contrecoup Brain Injury in Impact Induced TBI*. 2018. [Online]. Available: https://www.researchgate.net/publication/329554412

[12] M. B. Panzer, B. S. Myers, B. P. Capehart, and C. R. Bass, “Development of a finite element model for blast brain injury and the effects of CSF cavitation,” *Annals of Biomedical Engineering*, vol. 40, no. 7, pp. 1530–1544, Jul. 2012, doi: 10.1007/s10439-012-0519-2.

[13] J. Goeller, A. Wardlaw, D. Treichler, J. O’Bruba, and G. Weiss, “Investigation of cavitation as a possible damage mechanism in blast-induced traumatic brain injury,” *Journal of Neurotrauma*, vol. 29, no. 10, pp. 1970–1981, Jul. 2012, doi: 10.1089/neu.2011.2224.

[14] V. S. Caviness, D. N. Kennedy, C. Richelme, J. Rademacher, and P. A. Filipek, “The Human Brain Age 7-11 Years: A Volumetric Analysis Based on Magnetic Resonance Images.” [Online]. Available: https://academic.oup.com/cercor/article/6/5/726/497980

[15] C. H. Liu, Y. C. Lai, C. H. Chiu, and M. H. Lin, “Interior head impact analysis of automotive instrument panel for unrestrained front seat passengers,” in *Key Engineering Materials*, 2016, vol. 715, pp. 186–191. doi: 10.4028/www.scientific.net/KEM.715.186.

[16] K. Baeck, J. Goffin, and J. vander Sloten, “The use of different CSF representations in a numerical head model and their effect on the results of FE head impact analyses,” 2011.

[17] F. Wang *et al.*, “Prediction of brain deformations and risk of traumatic brain injury due to closed-head impact: quantitative analysis of the effects of boundary conditions and brain tissue constitutive model,” *Biomechanics and Modeling in Mechanobiology*, vol. 17, no. 4, pp. 1165–1185, Aug. 2018, doi: 10.1007/s10237-018-1021-z.

[18] Alan P. Bowling, “Vector Mechanics: A systematic Approach Third Edition”.

[19] Arthur Koster, “RELATING LINEAR AND ROTATIONAL ACCELERATIONS WITH INTERNAL PRESSURES DEVELOPED INSIDE HUMAN HEAD SURROGATE MODELS,” 2021.

[20] P. G. Young and C. L. Morfey, “INTRACRANIAL PRESSURE TRANSIENTS CAUSED BY HEAD IMPACTS.”

[21] P. G. Young, “An analytical model to predict the response of fluid-filled shells to impact - A model for blunt head impacts,” *Journal of Sound and Vibration*, vol. 267, no. 5, pp. 1107–1126, Nov. 2003, doi: 10.1016/S0022-460X(03)00200-1.

[22] S. J. RUAN, “Impact Biomechanics of Head Injury By Mathetmatical Modeling,” 1994.

[23] W. C. Moss, M. J. King, and E. G. Blackman, “Skull flexure from blast waves: A mechanism for brain injury with implications for helmet design,” *Physical Review Letters*, vol. 103, no. 10, Sep. 2009, doi: 10.1103/PhysRevLett.103.108702.